https://doi.org/10.48048/tis.2025.8764

Investigation of the Electrochemical Methylene Orange Effluent Degradation Using Graphite Battery Waste and Seawater

Gunawan Gunawan*, Nor Basid Adiwibawa Prasetya and Roni Adi Wijaya

Department of Chemistry, Diponegoro University, Semarang 50275, Indonesia

(*Corresponding author's e-mail: gunawan@live.undip.ac.id)

Received: 29 July 2024, Revised: 11 August 2024, Accepted: 17 August 2024, Published: 20 November 2024

Abstract

Electrochemical degradation using seawater and graphite electrodes from waste batteries for methylene orange (MO) dye degradation has been successfully carried out. Electrode characterization, electrolyte calibration, and dye degradation effectiveness with various voltages, pH, kinetics, and degradation reaction mechanisms were observed. Characterization showed a characteristic 2θ peak by X-ray diffractometer (XRD) at 26.5 °, and scanning electron microscopy-energy dispersive X-ray spectrometer (SEM-EDX) showed the morphology of hollow grains with carbon (C) and oxygen (O) composition. In addition, scanning potentiometry showed the initiation of hypochlorite compound formation and MO degradation. Further study of degradation effectiveness showed optimal results at 3 volts and above voltages. Hypochlorous acid (HOCl) and hypochlorite ions (OCl^-) from seawater are very effective oxidizing agents in acidic conditions compared to other pH conditions. Pseudo-first-order kinetics regulate the electron attack from the hypochlorite oxidizer (OCl^-), the hydroxyl groups (•OH) from the seawater electrolysis mechanism with graphite electrode media on the reactive groups, the ring binding on MO, and the degradation. This indicates that the graphite electrode system used to reuse waste batteries and seawater has the potential to degrade waste dyes in aquatic environments.

Keywords: Graphite battery waste, Seawater, Methylene orange

Introduction

The escalation in global energy demand has led to a significant increase in battery production and consumption, resulting in a surge in battery waste [1]. Graphite electrodes, among various waste components, pose a considerable challenge. These electrodes are often discarded in landfills [2]. Practical strategies for managing and recycling these materials are essential to reducing environmental impact. Other ecological problems, such as water pollution caused by synthetic dyes, have also been identified as critical environmental problems. Methylene orange, an artificial dye commonly used in the textile industry, is frequently detected in wastewater [3]. Synthetic dyes account for almost 800,000 tons annually; around 10 - 15 % is wasted in the textile industry [4]. These contaminants are known for their toxicity and persistence, making them challenging to degrade through conventional wastewater treatment methods. The presence of these pollutants in aquatic environments poses risks to human health and ecosystems, highlighting the urgent need for effective and sustainable treatment technologies [5].

Technology for dealing with organic pollutants and dye wastewater has evolved with several methods, including adsorption [6], coagulation [7,8], photocatalysis [9,10], ferrate [11,12], Advanced Oxidation Processes (AOPs) [13], Fenton modification [14], and electrochemical methods [15,16]. The advantages of electrochemistry are that it does not add additional pollutants to the environment, has shorter processing times, and effectively degrades dye waste.

The electrolyte and the type of electrode used influence the effectiveness of electrochemistry. The electrolyte used is usually an oxidizing salt solution such as sodium hydroxide (NaOH) [17], sodium chloride (NaCl) [18], sodium persulfate (Na_2SO_4) [19], and sodium hypochlorite (NaOCl) [20,21] obtained from

various sources. Sea water has excellent potential as an abundant, readily available, and economical source of electrolytes. Through the partial electrolysis process of NaCl in seawater, a mixed solution of seawater and chlorine compounds will be produced, which will react to form sodium hypochlorite, hydrogen gas, and hypochlorous acid, which plays a vital role as an oxidizer in electrolysis [22]. Meanwhile, electrode types have also been used, such as boron-doped diamond (BDD) Xu *et al.* [23] and SnO_2 Yu *et al.* [24], but they are very expensive, not commercially available, and less stable in large-scale processes. Carbon-based materials have been used as alternative electrode materials in biochemical degradation processes because they are superconductive, environmentally friendly, and non-toxic.

Research by Asghar *et al*. [25] studied a technique consisting of stainless steel and graphite electrodes for mineralizing the MB dye dissolved in water. The results revealed a maximum dye removal of up to 80 % with a 40-min operation time and a current density of 0.06 A/cm^2. Teng *et al*. [26] successfully used graphite and iron electrodes for 86 % degradation of MB dye. Meanwhile, this research aims to explore a new approach to tackle battery waste and water pollution by reusing spent graphite electrodes from used batteries for electrochemical degradation of methylene orange, which has never been done before. This research includes explicit electrode characterization, electrolyte calibration, and effectiveness of dye degradation with varying voltage, pH, kinetics, and degradation reaction mechanism. Reusing these electrodes is expected to provide a dual-benefit solution that can address waste management and water treatment challenges. In addition, this study investigated the use of seawater as an electrolyte in the degradation process. Seawater, an abundant and cost-effective resource, offers a sustainable alternative to conventional electrolytes used in electrochemical treatment.

Materials and methods

Materials and instrumentation

The materials used are seawater (Marina Beach, Semarang), battery electrode waste, acetate acid (CH_3COOH) (99 % purity, Merck, Germany), sodium persulphate (Na_2SO_4) (Merck, Germany), sodium hydroxide (NaOH) (Merck, Germany), aquadest, artificial waste methylene orange ($C_{14}H_{14}N_3NaO_3S$) (Merck, Germany) was prepared (1000 mg/L) and serial dilutions were made to obtain MB calibration, chloride acid (HCl) (Merck, Germany). While the instruments used are a Corr Test Potentiostat (CS-150) system with Ag/AgCl as reference electrode and Pt–wire counter electrode, a magnetic stirrer, a galvanostatic WYK-303B, Bruker D8 Advance X-ray diffractometer (XRD), JSM-6700F Analytical 20 kV scanning electron microscope (SEM), Swift ED3000 energy dispersive X-ray spectrometer (EDX), X-Ray fluorescence (XRF) Rigaku (RIX 3100), Bleach Test Kit (HI3843-Hanna Instruments), UV-Vis spectrophotometer (Genesys 10 S UV-Vis), LC-30A liquid chromatography (Shimadzu Co., Japan), and QTOF5600 mass spectrometry (AB Com., USA) with electrospray ionization source (EIS).

Preparation and characterization of electrodes

Graphite (C/C) electrodes were prepared by sonication of electrodes from spent batteries with ethanol and distilled water. Electrode characterization was performed with a JSM-6700F SEM-EDX cold-field emission scanning electron microscope to determine battery morphology and a Swift ED-3000 X-ray spectrometer (EDX) for compositional identification of surface content. Meanwhile, metal composition was confirmed using XRF analysis with a Rigaku wavelength dispersive X-ray fluorescence spectrometer (RIX 3100) equipped with a Rh X-ray tube, a 4-kW generator, and an 8-position crystal changer. In addition, XRD patterns were recorded using a Bruker D8 Advance X-ray diffractometer with Cu K radiation (λ = 1.5418). All electrode characterizations were observed to determine the differences in data before and after use in sewage treatment.

Calibration of electrolytes and samples

Calibration of seawater as electrolytes was scanned by scanning electrolysis from 0 - 8 volts using the CorrTest Potentiostat (CS-150) system with Pt and graphite electrodes using media 25 mL. On the other hand, artificial waste samples of methylene orange dye were calibrated with concentration variations of 5, 10, 15, 20, 25, 30, 35, 40, 45, and 50 mg/L. Calibration curves were obtained from spectrum and absorbance measurements made at the maximum wavelength with a UV-Vis spectrophotometer (Genesys 10 S UV-Vis).

Electrochemical degradation

Electrochemical degradation tests of dyes and antibiotics were carried out on an electrolytic cell under static galvanic conditions supplied by a WYK-303B galvanostatic. A batch reactor with a capacity of 250 mL was used for all electron-degradation studies. The anode and cathode were graphite plates of identical diameters. Graphite sheets of 2 by 4.5 by 0.3 cm were positioned in a parallel pattern, separated by 2 cm, and submerged in the sample solution to serve as the electrodes. 50 mg/L of previously calibrated methylene orange is the dye sample. Next, a steady 250 rpm stir was applied to the reactor. An analysis was conducted using a UV-Vis spectrophotometer to evaluate changes in the sample's absorbance value. While the spectra were being examined at a wavelength range of 200 - 600 nm, all operations were executed with the same protocol regarding sample variation.

Effect of parameter voltage and pH variation

The effect of voltage variation in the degradation of dyes and antibiotics was observed at an increase of every 1 volt in the range of 0 - 4 volts every constant time of 30 min. The effect of time on degradation efficiency was studied at various times of 0, 5, 10, 15, 20, 25, and 30 min with constant voltage conditions at the optimum value of each of the results of the previous voltage variation stage. Meanwhile, the pH parameter conditioning was carried out in neutral, acid, and alkali conditions. All resulting changes in dye concentration were measured by absorbance scanning using a UV-Vis spectrophotometer. Each electrochemical degradation efficiency and removal rate can be calculated by Eq. (1) [27]:

$$\text{Degradation efficiency (\%)} = [(A_0 - A_t) / A_0] \times 100\ \% \quad (1)$$

A_0 is the absorbance value in wavelength maximum (λ_{max}) of the initial waste sample (465 nm for MO), and A_t is the absorbance value at a given time t, respectively.

Determination of the kinetic and mechanism of the degradation pathway

Kinetic aspects were performed by preparing 20, 30, 40, 50, and 60 ppm MO with neutral pH treatment and 3-volt solution. Each concentration was observed for absorbance with a UV-Vis spectrophotometer with variations in degradation time of 5, 10, 15, 20, 25, and 30 min to observe the kinetics and reaction order. The electrochemical oxidation kinetics of MO were determined using a pseudo-first-order kinetic model, as expressed in Eq. (2), and the removal rates of MO were determined using the following Eq. (3) [28]:

$$-dC_t / dt = kC_0 \quad (2)$$

$$\eta = (C_0 - C_t) / C_0 \times 100\ \% \quad (3)$$

where C_0 is the initial concentration of MO before electrolysis (mg/L), C_t is the corresponding concentration at electrolysis time t (mg/L), and k (min^{-1}) is the pseudo-first-order rate constant. The kinetic parameters were calculated by fitting the experimental data with linear regression.

The dye degradation way was examined using QTOF5600 mass spectrometry (AB Com., USA) equipped with an electrospray ionization source (EIS) and LC-MS utilizing an LC-30A liquid chromatography (Shimadzu Co., Japan). MO 50 mg/L samples were utilized both pre- and post-treatment. The samples were pretreated using a high-speed cooled centrifuge (Tomy MX-200, Thermo Fisher Scientific) and a vortex mixer (Thermo Fisher Scientific, Waltham, MA, USA). However, the MassHunter B.07.00 workstation handles data processing. The limit of quantitation (LOQ) and limit of detection (LOD) were 100 and 10 mg/L, respectively, and the retention duration was recorded at 10 min.

Results and discussion

Characterization of electrodes

Characterization was performed to ascertain the viability of existing waste battery electrodes. Cu Kα radiation (1.54 Å) was used to collect X-ray diffraction data. **Figure 1** displays the findings of X-ray diffraction (XRD) investigations conducted throughout the 2θ range of 20 to 80 °. The rhombohedral graphite crystal planes (100) and (101) are indicated by the peaks at 2θ = 43.2 and 44.4 ° (JCPDS card No. 75-2078) [29]. The peaks at 2θ = 26.3 and 54.6 ° are attributed to the (002) and (004) graphite planes (JCPDS card No. 75-1621), respectively, whereas the peak at 2θ = 23.7 ° appears to be caused by the X-ray harmonics on the (002) graphite planes [30,31]. All peaks of the spent battery electrode

diffracted strongly and sharply, indicating that the obtained electrode is still well crystallized. The electro-degradation process did not change the location of the peaks; it only reduced their intensity.

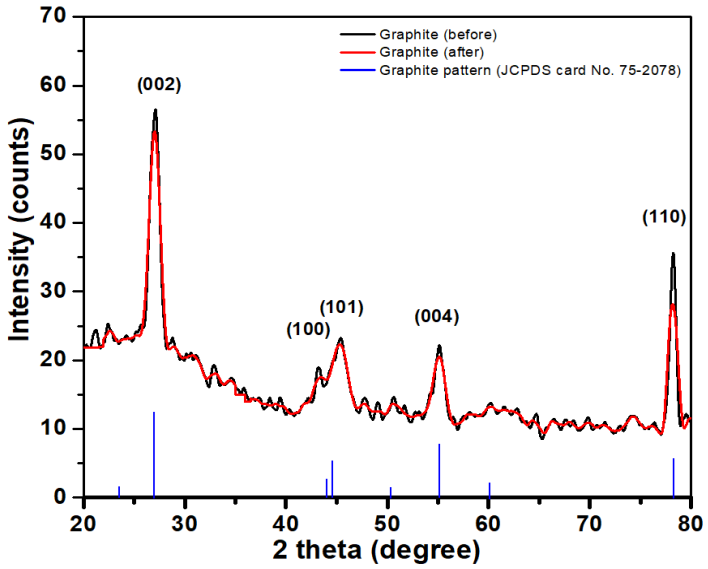

Figure 1 XRD patterns of graphite electrode before (fresh) and after (degraded).

Figure 2(**a**) and **2**(**b**) shows that the waste battery compartment consists of C and O elements. This is confirmed by SEM images showing nano-sized particles with a sponge-like structure [32]. The surface morphology of the graphite electrode has a granular shape with an observed grain size on the scale of 52.9 nm. The metal composition also follows the EDX analysis, namely O and C peaks. The graphite electrode before waste treatment consisted of 84.1 wt. % C and 11.9 wt. % oxygen, indicating that the waste battery still has the potential to be used as an electrode in degradation. On the other hand, after use, it consists of 58.1 wt. % C and 21.3 wt. % oxygen. Electrolysis indirectly produces a by-product in the form of oxygen attached to the surface of the electrode plane, so it is confirmed that there is an increase in oxygen content, which also fills the graphite scrapings, as shown in **Figure 2**(**b**).

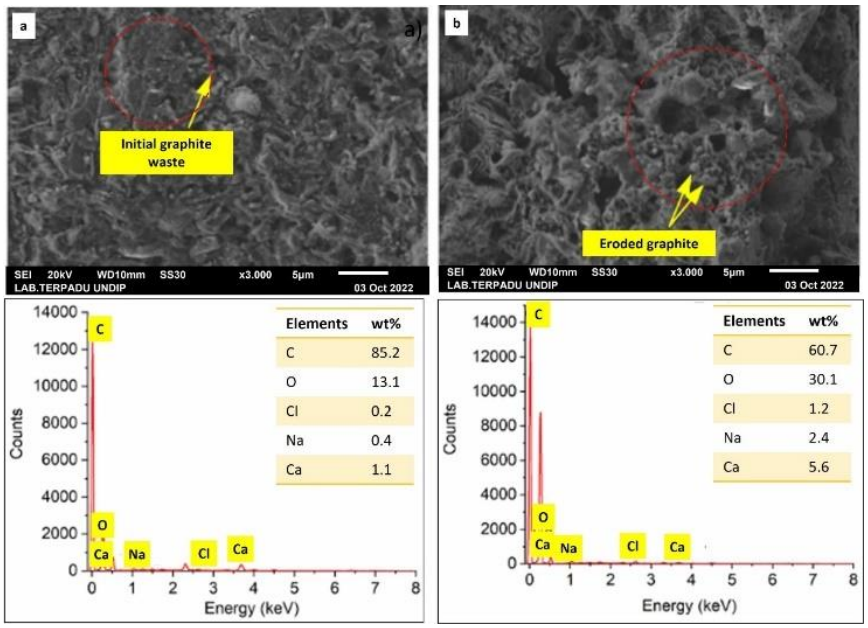

Figure 2 SEM-EDX images of graphite electrode surface before (a) and after (b) electrochemical degradation.

Calibration of electrolytes and samples

The seawater used as an electrolyte was scanned with an electrolysis potentiostat over a voltage range of 0 to 7 volts. This analysis aims to see seawater electrolysis's working potential range and trend. The process involves the decomposition of seawater into hydrogen and oxygen gas and the formation of chlorine if the electrolyte used is salt (NaCl), which is abundant in seawater. The current flowing in an electrolyte system at a given potential is recorded and plotted as a voltage versus current curve, as shown in **Figure 3**(**a**).

The curve shows an emerging current starting at 1.3 volts as a marker of reaction initiation and increasing sharply above 3 volts. In summary, in the range of 0 to 1.3 Volts, no seawater salt electrolysis occurs as it is below the required voltage. This corresponds to the theoretical minimum voltage for the decomposition of water (H_2O) into hydrogen (H_2) and oxygen (O_2), which is about 1.23 volts under standard conditions (25 °C, 1 atm) [33]. For graphite electrodes, overpotential by electrode resistance and electrochemical reaction efficiency at the anode and cathode can increase the voltage by about 0.5 to 1.0 Volt. Thus, this study's total potential current content to separate seawater into chlorine and salt with graphite electrodes is 2.5 or 3 volts and above [34]. At voltages around 1.3 to 2.5 V, the main product at the anode is oxygen (O_2). At voltages of 2.5 volt and above, especially if there is a significant concentration of chloride ions, chlorine (Cl_2) can form at the anode. While at the cathode, the main product is hydrogen (H_2) at various voltage ranges.

A more detailed reaction mechanism is based on potential standards, as shown in **Figure 3**(**b**). The reaction can overcome the activation energy barrier, close the insulating bubble, and produce a considerable reaction rate at a more significant potential difference (overpotential) between the 2 electrodes [15]. In addition, current must flow through the electrolytic circuit and the cell's electrical resistance to produce this potential difference. Based on Faraday's rule of electron equivalency, the seawater electrolysis process is a tried-and-true process. The more material oxidizes, the more positively it oxidizes. Consequently, hydrogen will develop at the cathode, and chlorine dioxide will be oxidized at the electrode's anode [35]. Thus, the overall reaction at the cathode and anode that occurs in seawater electrolysis is Eqs. (4) - (18).

Potential standard:

Cathode: $Na^+ (aq) + e^- \rightarrow Na^0 (s)$

E_0 red = −2.71 volt (4)

$2H_2O (l) + 2e^- \rightarrow H_2 (g) + 2OH^- (aq)$

E_0 red = −0.83 volt (5)

Anode: $2Cl^- (aq) \rightarrow Cl_2 (aq) + 2e^-$

E_0 oxidation = +1.36 volt (6)

$2H_2O (l) \rightarrow O_2 (g) + 4H^+ (aq) + 4e^-$

E_0 oxidation = +1.23 volt (7)

Electrolysis reaction:

(1.3 - 2.5 volt)

$2H_2O (l) \rightarrow O_2 (g) + 4H^+ (aq) + 4e^-$ (8)

$4H_2O (l) + 4e^- \rightarrow 2H_2 (g) + 4OH^- (aq)$ (9)

(2.5 - 3 volt)

$2Cl^- (aq) \rightarrow Cl_2 (aq) + 2e^-$ (10)

$2H_2O (l) + 2e^- \rightarrow H_2 (g) + 2OH^- (aq)$ (11)

(≥ 3 volt)

$Cl_2 (aq) + 2OH^- (aq) \rightarrow OCl^- (aq) + Cl^- (aq) + H_2O (aq)$ (12)

$H_2O (aq) \rightarrow H^+ (aq) + \bullet OH (aq) + e^-$ (13)

$OCl^- + H_2O \rightarrow HOCl + OH^- (aq)$ (14)

$HOCl (aq) \rightarrow Cl^- (aq) + \bullet OH (aq)$ (15)

$Na^+ (aq) + e^- \rightarrow Na^0 (s)$ (16)

(bulk stream)

$2Na^0 (s) + 2H_2O (l) \rightarrow 2NaOH (aq) + H_2 (aq)$ (17)

$HOCl (aq) + 2NaOH (aq) \rightarrow NaOCl (aq) + H_2O (aq)$ (18)

To produce hypochlorite, direct current (electricity) must be run through a NaCl solution (which separates into Na^+ and Cl^-). Chlorine gas (Cl_2) forms when the saltwater's dissolved salt (sodium chloride) is electrically charged. This gas is then quickly hydrolyzed to produce elemental sodium (Na0-no valency) and hypochlorous acid (HOCl) [36]. Hydroxide radicals (•OH) and active chlorine compounds (OCl^-) are created in subsequent reactions. Sodium hydroxide (NaOH) is created when sodium and water in the bulk stream react very quickly. When hypochlorous acid and sodium hydroxide combine, sodium hypochlorite (NaOCl) is

produced. Hydrogen gas is produced when salt and water mix. Hydrogen gas is a by-product of the gas phase since it does not react with other substances. At the cathode, cation reduction processes will produce hydrogen by electrolysis of seawater that contains sodium chloride (NaCl), acting as a natural catalyst.

The artificial dyes used were first calibrated to measure the accuracy of the actual absorbance with a UV-Vis spectrophotometer at the wavelength of maximum absorption. The analysis records transitions caused by the excitation of other electrons, providing information about the molecular electronic transitions occurring in this visible region. The observation results in **Figures 4(a)** and **4(b)** display the calibration data of MO dissolved in seawater at various concentrations of the same. The results show that the maximum wavelength of MO dissolved in seawater has a value of λ_{max} = 465 nm. All data showed good linearity with R^2 close to 1 (R^2 = 0.0991) with the reaction equation y = 0.0139x + 0.12738.

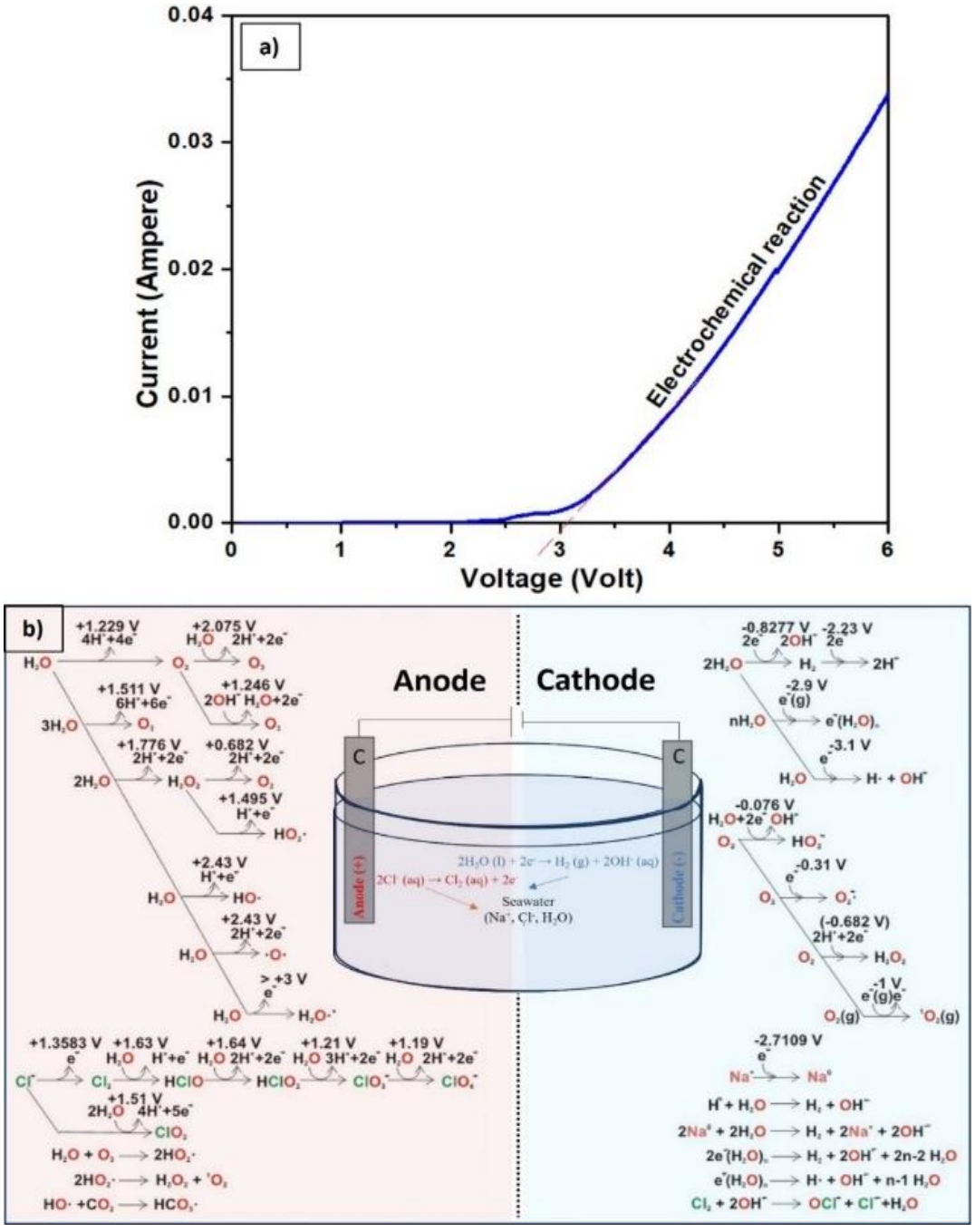

Figure 3 Seawater electrolysis scanning curve (a) and seawater electrolysis reaction mechanism (b).

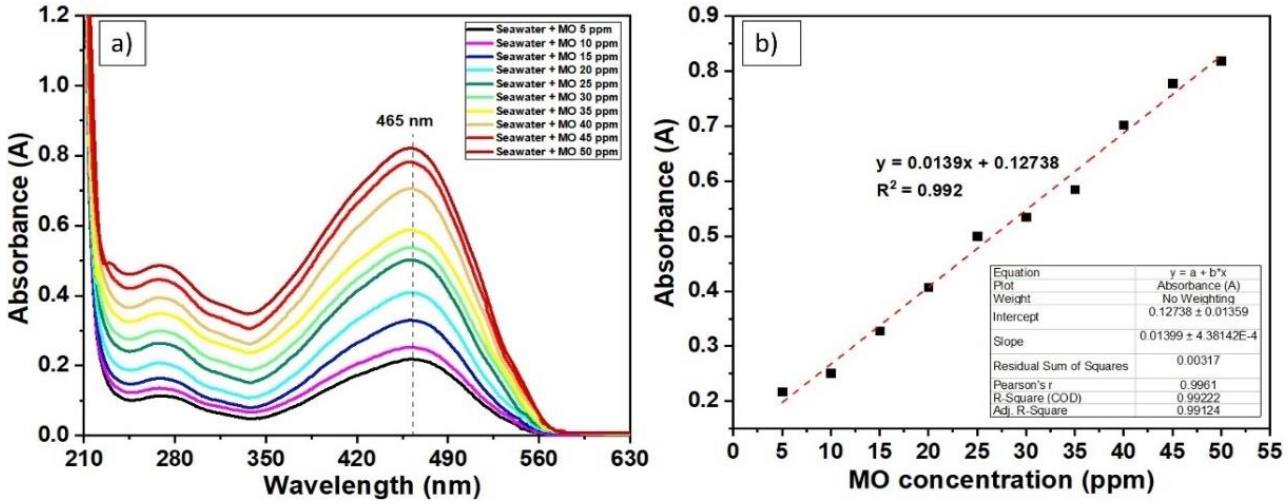

Figure 4 UV-Vis spectrum (a) and calibration curve (b) of methylene orange dissolved in seawater.

Electrochemical degradation

The electrochemical setup for MO degradation was set up as shown in **Figures 5(a)** and **5(b)**. The possible reactions in the electrolysis of dye wastewater using seawater electrolyte and graphite electrodes are shown in **Figure 5(a)**. The NaCl content in electrolysis acts as an excellent electrical conductor and is a source of chlorine that can degrade waste dyes and antibiotics so that their concentration is reduced. Salt, especially chloride ions, can undergo redox reactions on graphite electrodes. This electrolytic reaction can occur on the electrode to produce hypochlorite ion solutes (OCl^-, Cl^-), hydroxide radicals (•OH), and hydrogen gas [35] so that a more transparent solution is obtained, as in **Figure 5(c)**. These hypochlorite solutes can react with complex compounds to produce other materials. This study exploits its potential to decompose the complex compounds from dye effluents, which react with the dye complex compounds, as in Eqs. (19) - (25):

Anode (+): $2Cl^- \rightarrow Cl_2 + 2e^-$ (19)

$Cl_2 + 2OH^- \rightarrow H_2O + OCl^- + Cl^-$ (20)

$H_2O\ (aq) \rightarrow H^+\ (aq) + \bullet OH\ (aq) + e^-$ (21)

$OCl^- + H_2O \rightarrow HOCl + OH^-\ (aq)$ (22)

$HOCl\ (aq) \rightarrow Cl^-\ (aq) + \bullet OH\ (aq)$ (23)

Cathode (−): $2H_2O + 2e^- \rightarrow H_2 + 2OH^-$ (24)

Degradation reaction:

$C_{14}H_{14}N_3SO_3 + (HOCl/OCl^-$ atau $\bullet OH) \rightarrow CO_2 + H_2O + NO_3^- + SO_4^{2-}$ + other minerals (25)

Methyl Orange (MO) degradation in seawater electrolysis processes can occur through 2 main mechanisms: through reaction with active chlorine (Cl_2) and hydroxyl radicals (•OH). Both potent oxidizing agents can decompose organic compounds such as Methyl Orange. Active chlorine and its derivatives (HOCl and OCl^-) react with MO through oxidation [37]. The end products are usually fully oxidized compounds such as carbon dioxide (CO_2), water (H_2O), nitrogen oxides (NO_3^-), and sulfates (SO_4^{2-}). Hydroxyl radicals attack the chemical bonds in Methyl Orange, breaking the double bond in the azo structure (-N=N-) [38] and producing small compounds that can further oxidize to CO_2, H_2O, and other inorganic ions.

Effect of voltage variation

Figure 6 illustrates the impact of voltage on the dye's electrochemical degradation. The methylene orange absorption curve, depending on applied voltage variation, is displayed in **Figure 6(a)**. The difference in the initial pattern and after degradation with increasing voltage is a reaction symptom of seawater salt electrolysis. The apparent change in peak a (465 nm) is attributed to the azo structure of MO [39]. Because of the methyl orange's breakdown process at maximum absorption, this peak at 465 nm declines with increasing voltage. The reduced absorption at the maximum wavelength of MO is accompanied by a hypsochromic shift to the left, forming peak b at around 350 nm at 2.5 volts. This peak then fades and disappears entirely as the voltage increases. Meanwhile, peaks were observed at ~275 nm (peak d) and ~230 nm (peak c), which were

assigned to aromatic rings representing the products of simple compounds resulting from the degradation of MO molecules and the formation of chlorine compounds [40]. The peaks that emerge and vanish suggest 2 phases to the intermediate products produced in treating wastewater and electrochemically oxidizing MO. Initially, MO molecules undergo a disintegration phase, after which the smaller molecules undergo further electrochemical oxidation to provide the end products in the second step. In addition to the molecules breaking down, the azo structure is removed. The fact that the solution became transparent during the experiment, as seen in **Figure 5**(**c**), is supported by this outcome. The next difference also appears in the spectra results with treatment above 3 volts, which shows that the chlorine compound produced is too concentrated, as illustrated in the spectra of peaks c and d, due to the presence of hypochlorite (OCl^-) compound products from the electrolysis of seawater and graphite electrodes.

In **Figure 6**(**b**), in general, the degradation of the dye is directly proportional to the increase in the applied voltage from 0 - 3.5 volts. At voltages below 1.5 volts, a small portion of oxygen plays a role in degradation, as described in reactions 6 and 7. Then, the reaction increases sharply from 1.5 volts and above as a sign of exceeding the minimum voltage of electrolysis of water molecules to the peak of optimum potential degradation performance above 3.5 volt with almost 100 % degradation or 50 mg/L. At higher voltages, chloride ions in seawater can oxidize to chlorine gas (Cl_2), which can cause electrode corrosion and produce potentially harmful by-products. Inert electrodes such as platinum or graphite are typically used to prevent side reactions [41]. Chlorine (Cl_2) is generated at the anode at a high rate because chloride ions (Cl^-) are easily oxidized. At high voltages (3.0V to 5.0V), the formation of chlorine (Cl_2) becomes more significant, which can cause corrosion of the electrodes and generate harmful by-products. Therefore, voltage selection should be done carefully to avoid the formation of unwanted products and to ensure process efficiency. Thus, in this study, voltage 3 was used for further observation parameters

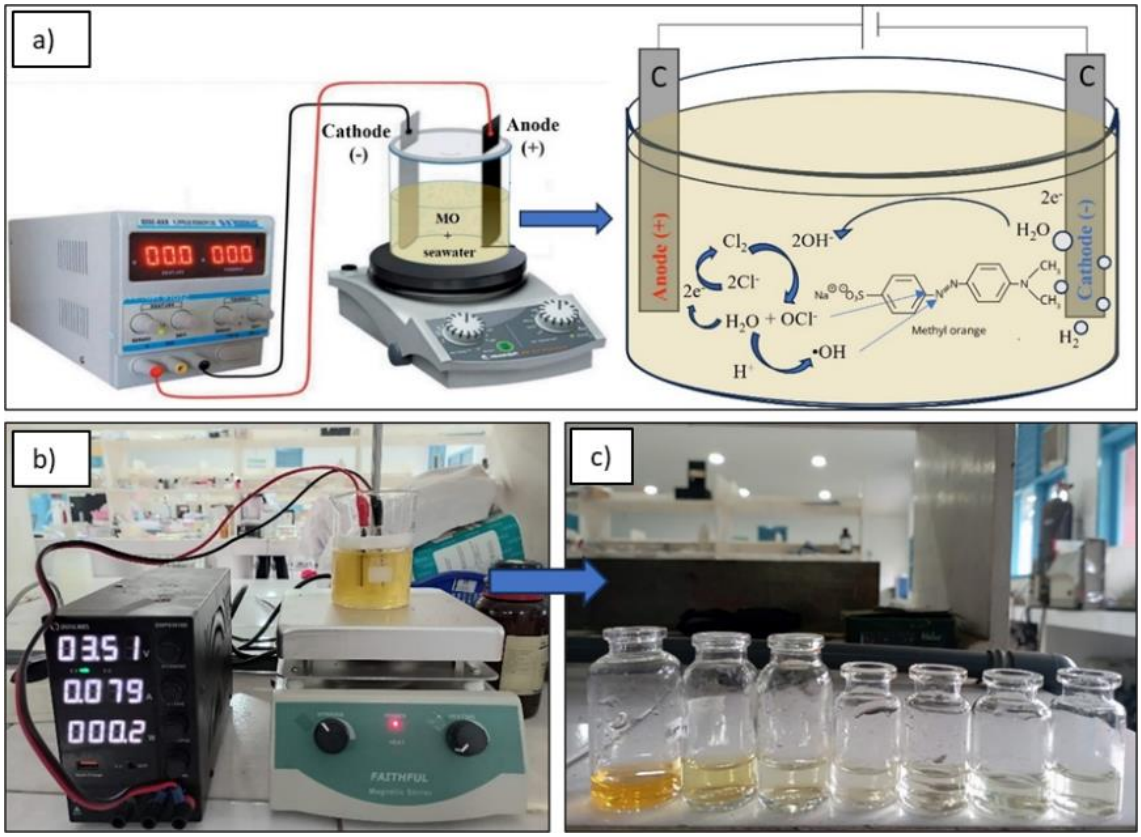

Figure 5 Electrochemical installation setup of MO degradation (a,b) and degradation results (c).

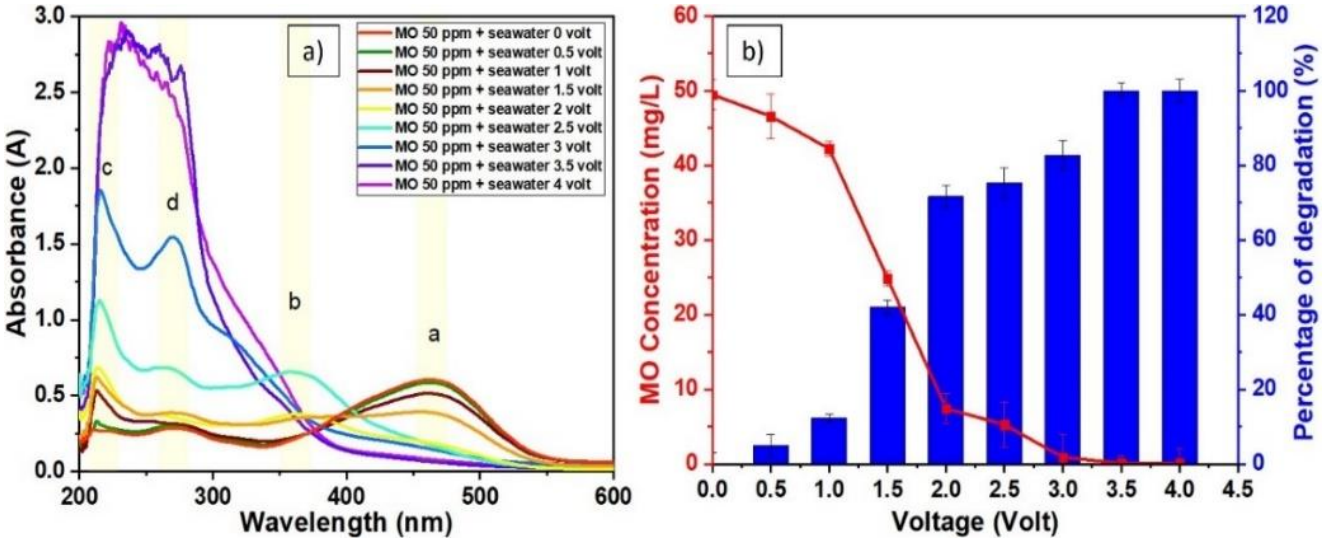

Figure 6 UV-Vis spectrum (a) and percentage decolorization (b) of MO with various voltages.

Effect of pH variation

The pH parameter affects the absorption and color of MO; this compound changes color from red in acidic conditions to yellow in alkaline conditions, as in **Figure 7**(**a**) - **7**(**e**). This color change is related to changes in the molecular structure of methyl orange, which is influenced by the pH of the solution [42]. As seen in **Figure 7**(**a**), In acidic conditions (low pH), methyl orange is in the protonated form ($[H\text{-}MO]^+$). This form absorbs light at a shorter wavelength, around 509 nm, which produces a red color in the solution. While under neutral to alkaline conditions (high pH), methyl orange turns into a deprotonated form (MO^-). This form absorbs light at a longer wavelength, around 465 nm, which produces a yellow color in solution. The color change of methyl orange occurs due to protonation and deprotonation of the azo (-N=N-) and sulfonate ($-SO_3H$) groups. The reaction can be explained by Eq. (26):

$$[H\text{-}MO] + \rightleftharpoons MO^- + H^+ \quad (26)$$

The UV-Vis spectra of methyl orange before and after degradation are greatly influenced by pH, as **Figures 7**(**b**) - **7**(**d**) demonstrates, since degradation results in changes to the molecule's chemical structure and the creation of degradation products. A sharp decrease in absorbance at λ_{max} corresponds to the structure of methyl orange (509 nm for the acidic form and 465 nm for the basic form) [43]. This decrease indicates that the original methyl orange concentration has been significantly reduced. The appearance of new peaks, for example, at 250 - 300 nm, indicates degradation products such as aniline or sulfanilic acid.

In addition, **Figure 7**(**e**) shows the trend that methyl orange degradation under acidic conditions is more effective, with an optimum yield of 100 % at 3 volts. This result occurs because hydrogen ions (H^+) can assist in the process of breaking the azo bond (-N=N-) to produce aniline, sulfanilic acid, or other small organic fragments such as aldehydes, carboxylic acids, and ketones more quickly. Chloride ions (Cl^-) in seawater can undergo oxidation to produce chlorine gas (Cl_2). This gas can subsequently react to produce hypochlorous acid (HOCl) and hypochlorite ions (OCl^-), both of which are highly effective oxidizing agents. **Figure 7**(**b**) illustrates that the typical hypochlorite absorption peak (275 nm) is significantly higher in acidic conditions than in other pH ranges. Methyl orange degradation can be less effective at high pH because hydroxide ions (OH^-) can neutralize specific degradation agents, producing more hydroxylated compounds. The hypochlorite ions (OCl^-) formed are more stable and less active at high pH, so it is possible to form chloride precipitates, which increase the absorbance over time, as shown in **Figure 7**(**d**).

A comparison of this study with several MO degradation methods is shown in **Table 1**. It can be seen that the effect of this method tends to have a better potent degradation efficiency than photocatalytic and ozonation. In addition, the reuse of waste battery electrode graphite and seawater also offers an easier method of preparation and degradation process.

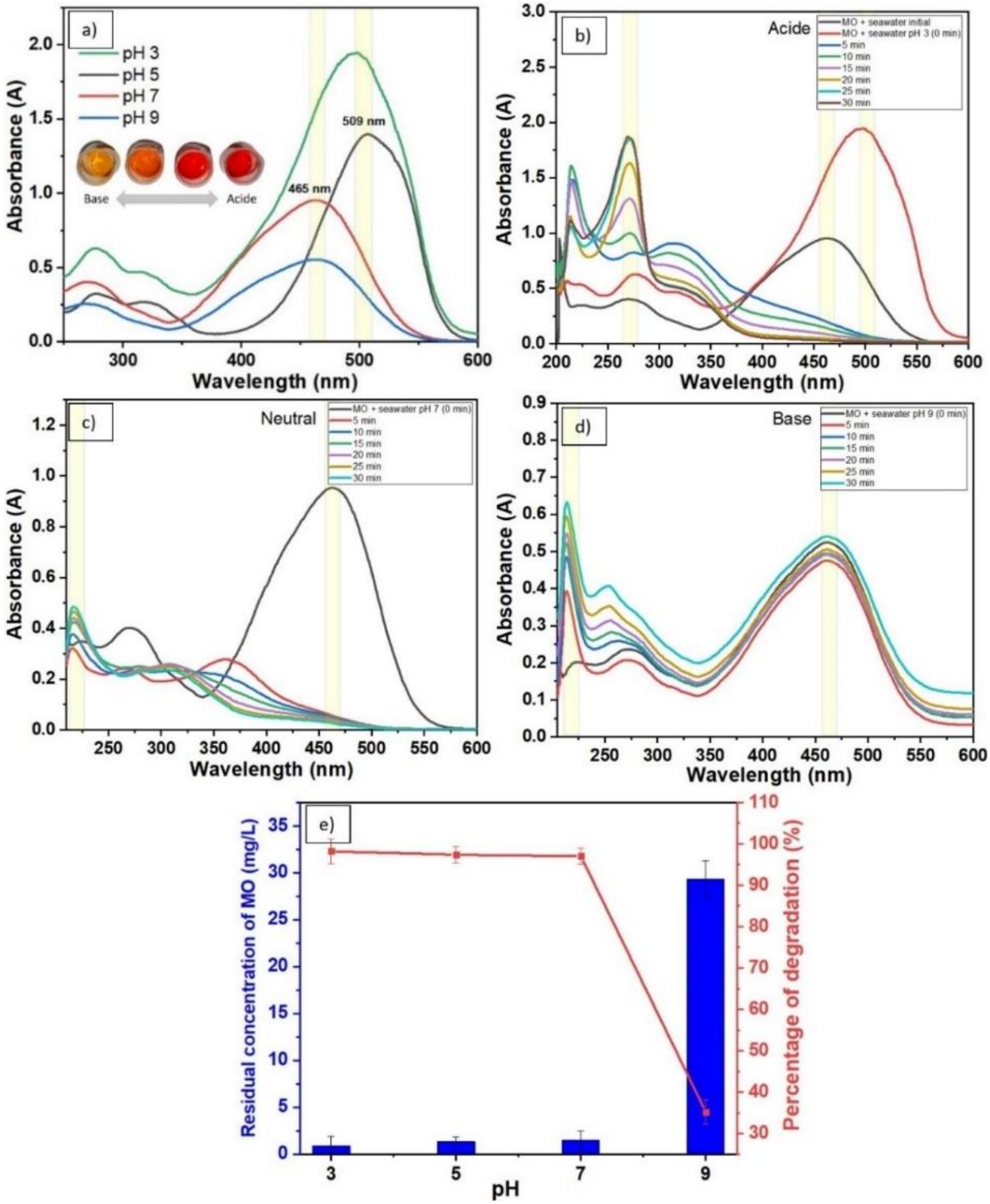

Figure 7 UV-Vis spectra of initial MO under acidic, essential, and neutral pH conditions (a), detailed spectra changes per time at acidic (b), neutral (c), and primary (d) pH, degradation percentage, and residual concentration of MO at various pH (e).

Table 1 Comparison of degradation efficiency by different methods.

Methods	Material	Degradation conditions	Degradation efficiency (%)	Ref.
Electro-degradation	Graphite battery waste	pH = 7, initial concentration = 50 mg/L, voltage = 3.5 volt, time = 30 min	100 %	This work
		pH = 3, initial concentration = 50 mg/L, voltage = 3 volt, time = 30 min	100 %	
Photocatalytic	MoS_2/Fe_3O_4	Initial concentration = 10 mg/L time = 100 min, under xenon lamp (300 W)	79.53 %	[44]
Photocatalytic	$Fe_3O_4@SiO_2@TiO_2@Ho$	Initial concentration = 3×10^{-5} M, time = 150 min, 400 W Hg lamp	78.4 %	[45]
Ozonation	$O_3/Fe^{2+}/S_2O_8^{2-}$	pH = 4, initial concentration = 200 mg/L, gas flow rate = 300 L/h	85 %	[46]

Determination of the kinetic and mechanism of degradation

Figure 8(**a**) illustrates that an increase in the starting dye concentration negatively impacts the clearance rate of MO. The clearance rates at 30, 40, 50, and 60 pm at starting concentrations were 89.3, 85.2, 80.8, and 78.7 % respectively. Furthermore, the connection of the apparent rate constant (k_c) and starting concentration was fitted using a pseudo-first-order kinetic model to examine the impact of the beginning concentration on the kinetic constant. According to **Figure 8**(**b**), when the initial concentration of MO increased, the pseudo-first-order kinetic constant (k) dropped. The experimental data was matched using linear regression to get the kinetic parameters. The values of k for various MO concentrations are, in order, 0.901×10^{-1}, 0.83×10^{-1}, 0.7×10^{-1}, and 0.59×10^{-1} min^{-1}. From 30 to 60 mg L^{-1} of starting MO concentration, it can be deduced that the values of k drop. This makes sense, as many intermediates are produced when organic contaminants are present in high concentrations and cannot be eliminated quickly enough. The active substance is also non-selective and, under some circumstances, has a constant production rate. This will restrict the interaction between active chemicals and MO molecules since many active substances will react with intermediates.

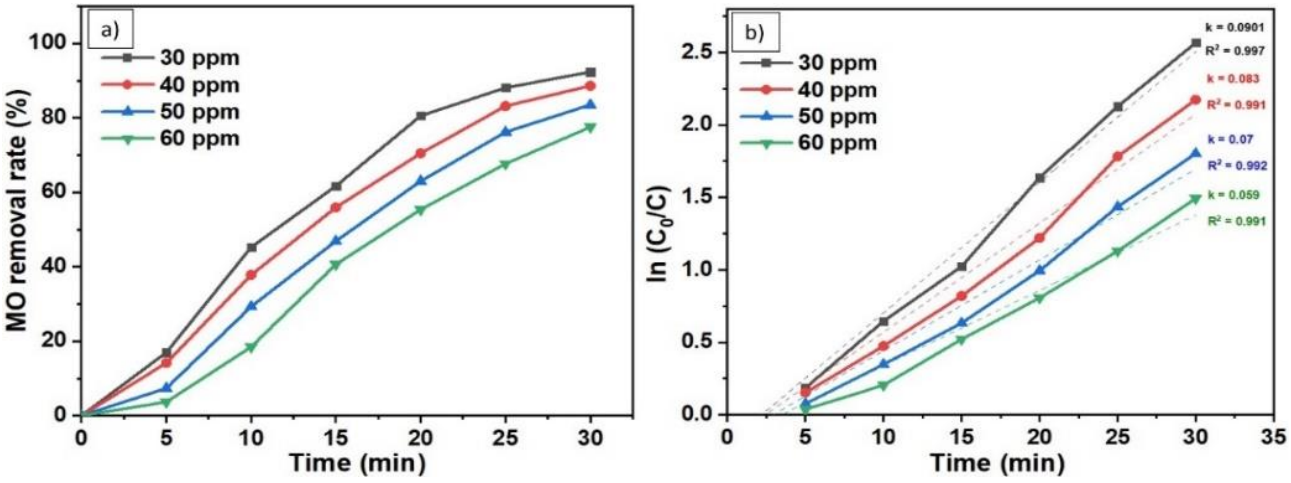

Figure 8 Removal rate (a) and pseudo-first-order kinetics fitting (b) of MO at various times.

The outcome can be interpreted in terms of the rates of electrochemical reactions and diffusion. The electrochemical reaction rate is higher than the diffusion rate at lower starting dye concentrations. Consequently, the electrode surface can be free of MO. More organic materials move to the surface of the electrode as the

starting concentration rises. The clearance rate will decline with increasing starting concentration because the produced •OH radicals are restricted [47].

The degradation reaction's intermediates were examined using LC/MS to learn more about the process of electrochemical degradation utilizing the graphite electrode and the seawater of MO that was the subject of this work (**Figure 9**). The azo group (-N=N-) in the structure of the molecules of MO functions as a chromophore, and because of concentration, the absorbance varies at the maximum wavelength. The hydroxyl (•OH) and chlorine radicals are produced by the following reaction when the decolorization process of MO is examined in an electrochemical device. To create nitrobenzene, the active ingredient (•OH) targets the massive conjugated structure of the azo link and benzene ring [48]. In the meantime, there's a MO decolorization response. An electrochemical oxidation process on the electrode surface can convert nitrobenzene molecules into phenolic compounds. When exposed to high oxidizing conditions, phenolic compounds undergo additional oxidation to produce quinones. According to studies, quinones can be converted to organic carboxylic acids. The organic molecule Cl element is changed into an anion, and its N element is changed into an anion or N_2. The products can finally be processed again to produce CO_2 and H_2O [49].

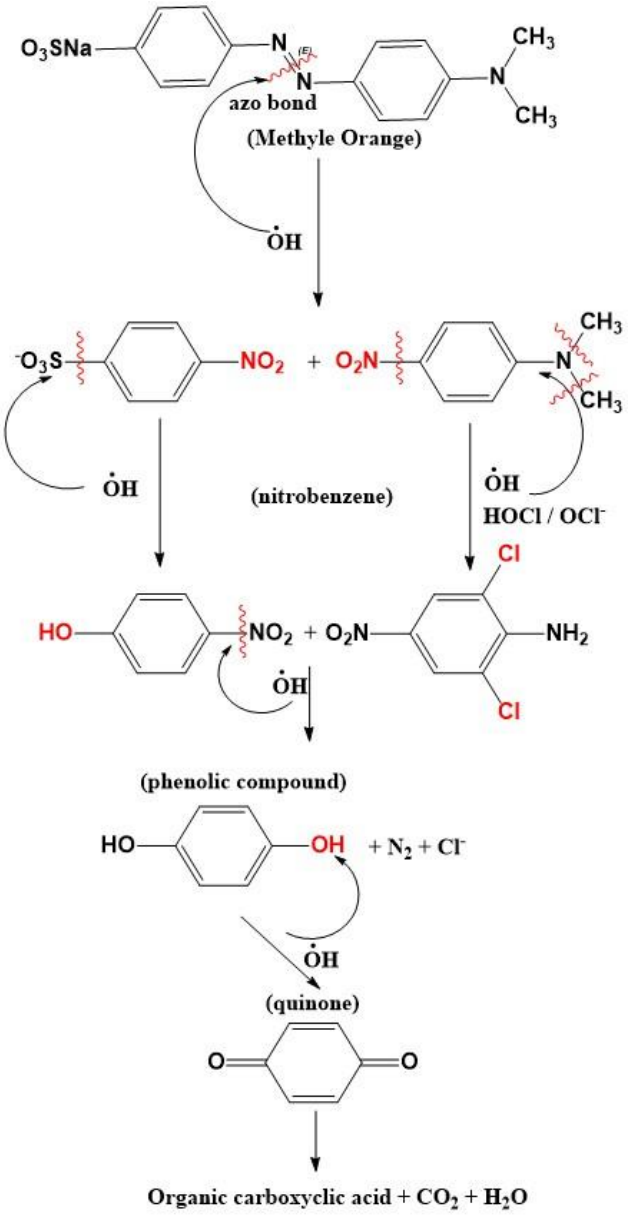

Figure 9 Mechanism of MO pathway degradation.

Conclusions

Electrochemical degradation using seawater and Graphite electrodes for dye waste treatment has been successfully conducted. The characterization revealed 2θ peaks at 26.5 °, supported by the graphite's properties as determined by XRD. The electrode's hollow granular morphology and carbon (C) and oxygen (O) composition matched the SEM-EDX. Scanning potentiometry demonstrated the beginning of the formation of hypochlorite compounds, which led to MO degradation in the range of 2.5 volts. Further study of degradation effectiveness showed optimal results at 3 volts and above voltages. Hypochlorous acid (HOCl) and hypochlorite ions (OCl^-) from seawater are very effective oxidizing agents in acidic conditions compared to other pH conditions. In general, the degradation of the dye is directly proportional to the increase in the applied voltage with almost 100 % degradation or 50 mg/L. The experimental data was matched using linear regression to get the kinetic parameters. Pseudo-first-order kinetics regulate the electron attack from the hypochlorite oxidizer (OCl^-), the hydroxyl groups (•OH) from the seawater electrolysis mechanism with graphite electrode media on the reactive groups, the ring binding on MO, and the degradation. This indicates that the graphite electrode system used to reuse waste batteries and seawater has the potential to degrade waste dyes in aquatic environments.

Acknowledgments

This research was funded by the Directorate of Resources, Directorate General of Higher Education, Ministry of Education, Culture, Research, and Technology Indonesia, with SPK No: 569-125/UN7.D2/PP/IV/2023.

References

[1] J Malinauskaite, L Anguilano and XS Rivera. Circular waste management of electric vehicle batteries: Legal and technical perspectives from the EU and the UK post Brexit. *International Journal of Thermofluids* 2021; **10**, 100078.

[2] EM Melchor-Martínez, R Macias-Garbett, A Malacara-Becerra, HMN Iqbal, JE Sosa-Hernandez and R Parra-Saldivar. Environmental impact of emerging contaminants from battery waste: A mini review. *Case Studies in Chemical and Environmental Engineering* 2021; **3**, 100104.

[3] BS Rathi, PS Kumar and DVN Vo. Critical review on hazardous pollutants in water environment: Occurrence, monitoring, fate, removal technologies and risk assessment. *Science of The Total Environment* 2021; **797**, 149134.

[4] B Pizzicato, S Pacifico, D Cayuela, G Mijas and M Riba-Moliner. Advancements in sustainable natural dyes for textile applications: A Review. *Molecules* 2023; **28(16)**, 5954.

[5] AL Ahmad, JY Chin, MHZM Harun and SC Low. Environmental impacts and imperative technologies towards sustainable treatment of aquaculture wastewater: A review. *Journal of Water Process Engineering* 2022; **46**, 102553.

[6] S Jiang, Y Lyu, J Zhang, X Zhang, M Yuan, Z Zhang, G Jin, B He, W Xiong and H Yi. Continuous adsorption removal of organic pollutants from wastewater in a UiO-66 fixed bed column. *Journal of Environmental Chemical Engineering* 2024; **12**(2), 111951.

[7] G Gunawan, A Haris, E Uswatun, S Glikeria and RA Wijaya. Study of methylene blue adsorption with silver chloride coagulants from photographic film waste. *Journal of Environment and Earth Science* 2022; **12(4)**, 54-62.

[8] RM El-taweel, N Mohamed, KA Alrefaey, S Husien, AB Abdel-Aziz, AI Salim, NG Mostafa, LA Said, IS Fahim and AG Radwan. A review of coagulation explaining its definition, mechanism, coagulant types, and optimization models; RSM, and ANN. *Current Research in Green and Sustainable Chemistry* 2023; **6**, 100358.

[9] S Mehra, J Saroha, E Rani, V Sharma, L Goswami, G Gupta, AK Srivastava and SN Sharma. Development of visible light-driven $SrTiO_3$ photocatalysts for the degradation of organic pollutants for waste-water treatment: Contrasting behavior of MB & MO dyes. *Optical Materials* 2023; **136**, 113344.

[10] MF Lanjwani, M Tuzen, MY Khuhawar and TA Saleh. Trends in photocatalytic degradation of organic dye pollutants using nanoparticles: A review. *Inorganic Chemistry Communications* 2024; **159**, 111613.

[11] Gunawan, NBA Prasetya and RA Wijaya. Electrochemical synthesis of ferrate (FeO_4^{2-}) in extreme alkaline medium and its application in dye degradation. *Asian Journal of Chemistry* 2022; **34(12)**, 3361-3368.

[12] Q Wang, Y Zhang, Y Yang, H Fu, Y Liang and J Ma. Zero valent copper-mediated ferrate (VI) for the degradation of bisphenol AF. *Journal of Environmental Chemical Engineering* 2023; **11**, 109600.

[13] G Gunawan, NBA Prasetya and RA Wijaya. Degradation of ciprofloxacin (CIP) antibiotic waste using the advanced oxidation process (AOP) method with ferrate (VI) from extreme base electrosynthesis. *Trends in Sciences* 2023; **20(7)**, 6639.

[14] DS Widodo, L Suyati, Gunawan, A Haris, RA Wijaya and SE Safitri. Modification of fenton method in decolorizing remazol black b via irradiationless approach using lead oxide. *AIP Conference Proceedings* 2022; **2553**, 020040.

[15] G Gunawan, NBA Prasetya, DS Widodo and RA Wijaya. Electrochemical degradation of methylene blue with seawater and Pb/PbO_2 electrodes from battery waste. *Karbala International Journal of Modern Science* 2023; **9(4)**, 725-741.

[16] MS Najafinejad, S Chianese, A Fenti, P Iovino and D Musmarra. Application of electrochemical oxidation for water and wastewater treatment: An overview. *Molecules* 2023; **28(10)**, 4208.

[17] T Liu, L Hao, Y Zhang, Y Hu, Q Zhao, Y Lu and X Ping. Anodized Bi_2O_3 film prepared in NaOH and oxalic acid and the photocatalytic activity in organic dye degradation. *Journal of Materials Science: Materials in Electronics* 2020; **31**, 10846-10854.

[18] R Antonelli, GRP Malpass, MGCD Silva and MGA Vieira. Photo-assisted electrochemical degradation of ciprofloxacin using DSA® anode with NaCl electrolyte and simultaneous chlorine photolysis. *Journal of Water Process Engineering* 2022; **47**, 102698.

[19] Z Frontistis, D Mantzavinos and S Meric. Degradation of antibiotic ampicillin on boron-doped diamond anode using the combined electrochemical oxidation - Sodium persulfate process. *Journal of Environmental Management* 2018; **223**, 878-887.

[20] G Gunawan, NBA Prasetya, A Haris and E Pratista. Ferrate synthesis using NaOCl and its application for dye removal. *Open Chemistry* 2022; **20(1)**, 1142-1154.

[21] FF Al-Qaim, ZH Mussa, MR Othman and MP Abdullah. Removal of caffeine from aqueous solution by indirect electrochemical oxidation using a graphite-PVC composite electrode: A role of hypochlorite ion as an oxidising agent. *Journal of Hazardous Materials* 2015; **300**, 387-397.

[22] L Sun, G Yang, X Cao and L Zhou. Photodegradation of methylene blue in natural seawater. *Journal of Ocean University of China* 2010; **9**, 135-138.

[23] T Xu, X Tang, M Qiu, X Lv, Y Shi, Y Zhou, Y Xie, M Naushad, SS Lam, HS Ng, C Sonne and S Ge. Degradation of levofloxacin from antibiotic wastewater by pulse electrochemical oxidation with BDD electrode. *Journal of Environmental Management* 2023; **344**, 118718.

[24] H Yu, X Zhang, M Zhao, L Zhang, H Dong and H Yu. Norfloxacin degradation by a green carbon black-Ti/SnO_2-Sb electrochemical system in saline water. *Catalysis Today* 2019; **327**, 308-314.

[25] A Asghar, AAA Raman and WMAW Daud. Advanced oxidation processes for in-situ production of hydrogen peroxide/hydroxyl radical for textile wastewater treatment: A review. *Journal of Cleaner Production* 2015; **87**, 826-838.

[26] X Teng, J Li, Z Wang, Z Wei, C Chen, K Du, C Zhao, G Yang and Y Li. Performance and mechanism of methylene blue degradation by an electrochemical process. *RSC Advances* 2020; **10(41)**, 24712-24720.

[27] SF Deriase, RA El-Salamony, E Amdeha and AM Al-Sabagh. Statistical optimization of photocatalytic degradation process of methylene blue dye by SnO–TiO_2–AC composite using response surface methodology. *Environmental Progress & Sustainable Energy* 2021; **40(5)**, e13639.

[28] G Wang, Y Liu, J Ye, Z Lin and X Yang. Electrochemical oxidation of methyl orange by a Magnéli phase Ti_4O_7 anode. *Chemosphere* 2020; **241**, 125084.

[29] A Shalaby, D Nihtianova, P Markov, AD Staneva, RS Iordanova and YB Dimitriev. Structural analysis of reduced graphene oxide by transmission electron microscopy. *Bulgarian Chemical Communications* 2015; **47(1)**, 291-295.

[30] T Luo, J Liu, L Chen, S Zeng and Y Qian. Synthesis of helically coiled carbon nanotubes by reducing ethyl ether with metallic zinc. *Carbon* 2005; **43(4)**, 755-759.

[31] SMS Al-Mufti, A Almontasser and SJA Rizvi. Single and double thermal reduction processes for synthesis reduced graphene oxide assisted by a muffle furnace: A facile robust synthesis and rapid approach to enhance electrical conductivity. *AIP Advances* 2022; **12(12)**, 125306.

[32] A Ahmed, A Hayat, MH Nawaz, P John and M Nasir. Construction of sponge-like graphitic carbon nitride and silver oxide nanocomposite probe for highly sensitive and selective turn-off fluorometric detection of hydrogen peroxide. *Journal of Colloid and Interface Science* 2020; **558**, 230-241.

[33] C Saleh and B Romadhon. Design and build of hydrogen production prototype using water electrolysis method using solar panels. *International Journal of Scientific Engineering and Science* 2022; **6(2)**, 72-77.

[34] AA Afify, GK Hassan, HE Al-Hazmi, RM Kamal, RM Mohamed, J Drewnowski, J Majtacz, J Mąkinia and HA El-Gawad. Electrochemical production of sodium hypochlorite from salty wastewater using a flow-by porous graphite electrode. *Energies* 2023; **16(12)**, 4754.

[35] G Amikam, P Nativ and Y Gendel. Chlorine-free alkaline seawater electrolysis for hydrogen production. *International Journal of Hydrogen Energy* 2018; **43(13)**, 6504-6514.

[36] N Janudin, NAM Kasim, VF Knight, NA Halim, SAM Noor, KK Ong, WMZW Yunus, MNF Norrrahim, MSM Misenan, MAIA Razak, MZ Ahmad and MH Yaacob. Sensing techniques on determination of chlorine gas and free chlorine in water. *Journal of Sensors* 2022; **2022**, 1898417.

[37] M Deborde and UV Gunten. Reactions of chlorine with inorganic and organic compounds during water treatment-Kinetics and mechanisms: A critical review. *Water Research* 2008; **42(1-2)**, 13-51.

[38] PCW Cheung, DR Williams, DW Kirk, PJ Murphy, SJ Barton and J Barker. Decolourisation of metal-azo dyes in wastewaters by sodium peroxodi sulphate: A Template for experimental investigations. *The Open Environmental Research Journal* 2023; **16**, e259027762301240.

[39] DAE Mously, AM Mahmoud, MM Gomaa and HZ Yamani. Rapid catalytic reduction of environmentally toxic azo dye pollutant by Prussian blue analogue nanocatalyst. *RSC Advances* 2024; **14**, 15232-15239.

[40] LG Devi, SG Kumar, KM Reddy and C Munikrishnappa. Photo degradation of methyl orange an azo dye by advanced fenton process using zero valent metallic iron: Influence of various reaction parameters and its degradation mechanism. *Journal of Hazardous Materials* 2009; **164(2-3)**, 459-467.

[41] H Saada, B Fabre, G Loget and G Benoit. Is direct seawater splitting realistic with conventional electrolyzer technologies? *ACS Energy Letters* 2024; **9(7)**, 3351-3368.

[42] MF Hanafi and N Sapawe. Influence of pH on the photocatalytic degradation of methyl orange using nickel catalyst. *Materials Today: Proceedings* 2020; **31(1)**, 339-341.

[43] J Zhang, Q Liu, Y Chen, Z Liu and C Xu. Determination of acid dissociation constant of methyl red by multi-peaks Gaussian fitting method based on UV-visible absorption spectrum. *Acta Physica Sinica* 2012; **28(5)**, 1030-1036.

[44] X Lin, X Wang, Q Zhou, C Wen, S Su, J Xiang, P Cheng, X Hu, Y Li, X Wang, X Gao, R Nozel, G Zhou, Z Zhang and J Liu. Magnetically recyclable MoS_2/Fe_3O_4 hybrid composite as visible light responsive photocatalyst with enhanced photocatalytic performance. *ACS Sustainable Chemistry & Engineering* 2019; **7(1)**, 1673-1682.

[45] S Mortazavi-Derazkola, M Salavati-Niasari, O Amiri and A Abbasi. Fabrication and characterization of $Fe_3O_4@SiO_2@TiO_2@Ho$ nanostructures as a novel and highly efficient photocatalyst for degradation of organic pollution. *Journal of Energy Chemistry* 2017; **26(1)**, 17-23.

[46] D Ge, Z Zeng, M Arowo, H Zou, J Chen and L Shao. Degradation of methyl orange by ozone in the presence of ferrous and persulfate ions in a rotating packed bed. *Chemosphere* 2016; **146**, 413-418.

[47] Y Zhao, J Cui, S Sarrouf, S Hojabri and AN Alshawabkeh. Degradation of Ibuprofen in flow-through system by the electro-fenton process activated by two iron sources, Available at: https://doi.org/10.21203/rs.3.rs-2608922/v1, accessed May 2021.

[48] Z Zhang, G Wang, W Li, L Zhang, T Chen and L Ding. Degradation of methyl orange through hydroxyl radical generated by optically excited biochar: Performance and mechanism. *Colloids and Surfaces A: Physicochemical and Engineering Aspects* 2020; **601**, 125034.

[49] M Saeed, S Adeel, M Ilyas, MA Shahzad, M Usman, EU Haq and M Hamayun. Oxidative degradation of Methyl Orange catalyzed by lab prepared nickel hydroxide in aqueous medium. *Desalination and Water Treatment.* 2016; **57(27)**, 12804-12813.